

Modeling the effects of vasculature evolution on early brain tumor growth

Jana L. Gevertz^a, Salvatore Torquato^{a,b,c,d,*}

^a*Program in Applied and Computational Mathematics, Princeton University, Princeton, NJ 08544, USA*

^b*Department of Chemistry, Princeton University, Princeton, NJ 08544, USA*

^c*Princeton Institute for the Science and Technology of Materials, Princeton University, Princeton, NJ 08544, USA*

^d*Princeton Center for Theoretical Physics, Princeton University, Princeton, NJ 08544, USA*

Received 16 March 2006; received in revised form 9 June 2006; accepted 6 July 2006

Available online 15 July 2006

Abstract

Mathematical modeling of both tumor growth and angiogenesis have been active areas of research for the past several decades. Such models can be classified into one of two categories: those that analyze the remodeling of the vasculature while ignoring changes in the tumor mass, and those that predict tumor expansion in the presence of a non-evolving vasculature. However, it is well accepted that vasculature remodeling and tumor growth strongly depend on one another. For this reason, we have developed a two-dimensional hybrid cellular automaton model of early brain tumor growth that couples the remodeling of the microvasculature with the evolution of the tumor mass. A system of reaction–diffusion equations has been developed to track the concentration of vascular endothelial growth factor (VEGF), Ang-1, Ang-2, their receptors and their complexes in space and time. The properties of the vasculature and hence of each cell are determined by the relative concentrations of these key angiogenic factors. The model exhibits an angiogenic switch consistent with experimental observations on the upregulation of angiogenesis. Particularly, we show that if the pathways that produce and respond to VEGF and the angiopoietins are properly functioning, angiogenesis is initiated and a tumor can grow to a macroscopic size. However, if the VEGF pathway is inhibited, angiogenesis does not occur and tumor growth is thwarted beyond 1–2 mm in size. Furthermore, we show that tumor expansion can occur in well-vascularized environments even when angiogenesis is inhibited, suggesting that anti-angiogenic therapies may not be sufficient to eliminate a population of actively dividing malignant cells.

© 2006 Elsevier Ltd. All rights reserved.

Keywords: Angiogenesis; Angiopoietin; VEGF; Tumor growth; Hybrid cellular automaton

1. Introduction

Cancer biology has been revolutionized over the past several decades. Genetic alterations that lead to malignant phenotypes have been identified (Hulleman and Helin, 2005; Maher et al., 2001), and mechanisms necessary to sustain a solid tumor (i.e. angiogenesis) (Brat et al., 2003; Folkman, 2003; Holash et al., 1999a,b) and that contribute to tumor–cell invasion (Giese and Manfred, 1996; Visted

et al., 2003) have been elucidated. These advances in cancer biology have greatly improved the prognosis of individuals diagnosed with many cancer types, but glioblastoma multiforme (GBM) is not one of them (Maher et al., 2001). GBM is the most aggressive of the gliomas, a collection of tumors arising from the glial cells or their precursors in the central nervous system (Holland, 2000). Despite advances made in cancer biology, the median survival time for a patient diagnosed with GBM is only 8 months, a fact that has changed little over the past several decades (Maher et al., 2001).

The following question naturally arises: what is unique about GBM that enables it to evade all attempts at treatment? The answer to this question can be found in the tumor name itself. GBM is a multiforme, meaning it is

*Corresponding author. Department of Chemistry, Princeton University, Princeton, NJ 08544, USA. Tel.: +1 609 258 3341; fax: +1 609 258 6746.

E-mail addresses: torquato@princeton.edu,
torquato@electron.princeton.edu (S. Torquato).

complex at many levels of organization (Holland, 2000). GBM exhibits diversity at the macroscopic level, having necrotic, hypoxic and proliferative regions. At the mesoscopic level, tumor–cell interactions, microvascular remodeling (Holash et al., 1999a) and pseudopalisading necrosis are observed (Brat et al., 2004). Further, the discovery that tumor stem cells may be the sole malignant cell type with the ability to proliferate, self-renew and differentiate introduces yet another level of mesoscopic complexity to GBM (Singh et al., 2004a,b). At the microscopic level, GBM cells can exhibit a variety of point mutations, chromosomal deletions and chromosomal amplifications (Holland, 2000).

In order to understand how GBM thrives in spite of therapeutic attempts to undermine growth, one must study the interactions that occur in GBM at different length scales (Hatzikirou et al., 2005); for example, how a point mutation can affect microvascular remodeling, which in turn affects tumor size, shape and composition. The most logical way to study the interaction of processes at multiple length scales is via a mathematical model that can integrate phenomena occurring at the macroscopic/tissue scale, mesoscopic/cellular scale and microscopic/genetic scale (Alarcón et al., 2005; Hatzikirou et al., 2005; Zheng et al., 2005). Only by integrating the processes that occur at each scale can we truly understand the evolution of a GBM mass, and why GBM responds poorly to therapeutic efforts.

While many events contribute to the growth properties of a neoplasm, in this paper we choose to focus on how the microscopic and mesoscopic properties of the microvasculature affect the expansion of the tumor. To achieve this goal, an understanding of how the microvasculature evolves is required. Until recently, it was widely accepted that solid tumor growth is divided into three stages: avascular growth in which the tumor receives its nutrients and oxygen via its surface, angiogenesis, which leads to the formation of new blood vessels that eventually vascularize the tumor, and vascular growth, when the tumor has established its own blood supply (Alarcón et al., 2005).

Recent evidence suggests, however, that tumors arising in vascularized tissue such as the brain do not originate avascularly (Holash et al., 1999a,b). Instead, it is hypothesized that glioma growth is a process involving vessel co-option, regression and growth. Three key proteins, vascular endothelial growth factor (VEGF) and the angiopoietins, angiopoietin-1 (Ang-1) and angiopoietin-2 (Ang-2), are required to mediate these processes (Holash et al., 1999a,b).

VEGF is a hypoxia-inducible 38–46 kDa glycoprotein, which is a ligand for the endothelial cell (EC)-specific tyrosine kinase receptors VEGFR-1/Flt-1 and VEGFR-2/Flk-1 (Brekken and Thorpe, 2001). VEGF functions as a potent permeability-inducing agent, an EC chemotactic agent, an EC proliferative factor and an anti-apoptotic signal for ECs (Brekken and Thorpe, 2001). While VEGF binds to both VEGFR-1 and VEGFR-2 with high affinity,

the VEGF-VEGFR-2 pathway appears to be responsible for vascular permeability, and hence has been strongly implicated as the dominant signal transduction pathway in tumor angiogenesis (Brekken and Thorpe, 2001).

While VEGF is responsible for the formation of an immature vascular network, VEGF is unable to stabilize the newly formed vessels. This is where Ang-1 comes into play. Ang-1 is a ligand for the EC-specific receptor tyrosine kinase Tie-2. The binding of Ang-1 to Tie-2 mediates interactions between ECs and surrounding support cells, resulting in the *maturation* and *stabilization* of immature blood vessels.

A natural antagonist of Ang-1, Ang-2, was identified shortly after the discovery of Ang-1 (Maisonpierre et al., 1997). Unlike the constitutively expressed Ang-1, Ang-2 is expressed only at sites of vascular remodeling. Since Ang-2 competes with Ang-1 for Tie-2 binding, Ang-2 is responsible for the *destabilization* of the vasculature. The action of Ang-2 depends on VEGF: in the presence of VEGF, a strong angiogenic response is triggered by Ang-2 plus VEGF, while in the absence of VEGF, Ang-2 expression results in vessel regression (Holash et al., 1999a,b).

We can now paint a picture of what likely occurs during the process of glioma vascularization. As a malignant mass grows, the tumor cells co-opt the mature vessels of the surrounding brain that express constant levels of bound Ang-1. Vessel co-option leads to the upregulation in Ang-2 and this shifts the ratio of bound Ang-2 to bound Ang-1. In the absence of VEGF, this shift destabilizes the co-opted vessels within the tumor center and marks them for regression (Holash et al., 1999b; Maisonpierre et al., 1997). Vessel regression in the absence of vessel growth leads to the formation of hypoxic regions in the tumor mass. Hypoxia induces the expression of VEGF, stimulating the growth of new blood vessels (Secomb et al., 2000). This robust angiogenic response eventually rescues the suffocating tumor. Glioma growth dynamics remain intricately tied to the continuing processes of vessel co-option, regression and growth.

Angiogenesis is a topic that has lent itself to much mathematical modeling over the past several years (Anderson and Chaplain, 1998; Hahnfeldt et al., 1999; Levine et al., 2001; McDougall et al., 2006; Plank et al., 2004; Scalerandi et al., 2001; Scalerandi and Sansone, 2002). The majority of existing angiogenic models aim to describe the evolution of ECs in response to tumor stimuli. A particularly relevant set of angiogenic models has been generated by Chaplain et al. (Anderson and Chaplain, 1998; McDougall et al., 2006). In these models, many important features of the angiogenic process, including the diffusion of ECs, chemotaxis of ECs along tumor angiogenic factor gradients, haptotaxis of ECs along fibronectin gradients and blood flow through the network, are explicitly accounted for in order to predict the architecture of a tumor-induced capillary network. The authors showed that the morphology of tumor capillary networks generated by their model is consistent with the

structure of tumor-induced capillary networks observed in vivo (McDougall et al., 2006). While this family of detailed angiogenic models predicts well the structure of tumor-associated capillary networks, the tumor in this model acts as nothing more than a constant source that provides the capillary network with the chemicals it needs to evolve. However, it is well established that tumor growth and vascular remodeling are strongly linked; that is, changes in the tumor cause changes in the vasculature, and changes in the vasculature cause changes in the tumor. While almost all angiogenic models ignore the feedback that occurs between a growing tumor and the microvasculature, an exception to this is the work by Scalerandi and Sansone (2002). In this model, the physical and biological interactions between the tumor and the vasculature are used to describe the avascular–vascular transition. While this model is similar to ours in that it accounts for the feedback between tumor growth and angiogenesis, a different biological model of tumor vascularization is assumed.

We have developed a novel model that considers the interdependence of vascular remodeling and tumor growth. This model has its origin in a cellular automaton (CA) model developed by Kansal et al. (2000a), in which it was shown that three-dimensional tumor growth and composition can be realistically predicted by four microscopic parameters that account for the nutritional needs of the tumor, cell-doubling time and the mechanical confinements of the brain. The original model was used as the basis for a second study, in which a distinct subpopulation was introduced into a homogeneous tumor, and the growth dynamics of the resulting heterogeneous tumor were analyzed (Kansal et al., 2000a). This study showed that subpopulations with very small growth advantages have a finite probability of “emergence”; i.e. surviving for an extended period of time. The emergence of even one such subpopulation was shown to drastically alter tumor growth dynamics, suggesting that prognosis based on the assumption of a monoclonal tumor can be markedly inaccurate (Kansal et al., 2000b). Finally, the CA model has been applied to study the effects that surgical removal followed by chemotherapy have on the evolution of a homogeneous and heterogeneous GBM mass (Schmitz et al., 2002). This study concluded that the spatial distribution of chemotherapeutic resistant cells is an important indicator of tumor survival and growth. Particularly, when resistant cells are not confined to a particular location, patient prognosis is significantly worse than when resistant cells are localized in the neoplasm. It was also shown that the shape of the reoccurring tumor depends on the rate at which chemotherapy induces mutations (Schmitz et al., 2002). While these three studies were successful at analysing homogeneous and heterogeneous GBM growth both with and without treatment, in each case, the model made the oversimplifying assumption that the tumor mass is well-vascularized. In other words, both the vascular network and angiogenesis are implicitly present in these models. In order to increase the microscopic detail of the model, we

propose a two-dimensional hybrid variant of the original CA model that allows us to study how changes in the tumor vasculature due to vessel co-option, regression and sprouting influence GBM development.

A CA model is ideally suited for studying GBM growth dynamics. The discrete nature of actual cells are realistically captured in a CA model. By treating cells in a discrete fashion, we can capture the fact that each tumor cell has unique properties that do not continuously depend on their neighbors. In other words, the heterogeneous nature of a GBM mass is easily realized in a discrete CA model (Kansal et al., 2000a). Furthermore, due to the complex nature of GBM, the mechanisms that control its dynamics are not fully understood. In order to describe GBM growth using a CA model, one only needs to attempt to mimic the physical laws that govern tumor growth by using a simple set of local rules.

The model presented here retains several important features of the original algorithm. These include:

- The use of the Voronoi tessellation to study the dynamics of tumor growth.
- The classification of tumor cells into three distinct types: proliferative cells, non-proliferative/hypoxic cells and necrotic cells.
- The inclusion of mechanical confinement pressure to simulate physiological confinement by the skull.

Key differences also exist between the current and previous models. In the original models, tumor growth occurred in three spatial dimensions, and it was assumed that the tumor was well-vascularized. In the new model, growth occurs in two spatial dimensions, but we explicitly account for vascularization. The two-dimensional results from this model can be thought of as a cross-central section of a spherical tumor. The original model also used an adaptive lattice to simulate brain tumor growth over several orders of magnitude. In the adaptive lattice, the automaton cells closest to the lattice center represented roughly 100 biological cells, while the outermost cells represented roughly 10^6 real cells (Kansal et al., 2000a). In the current version of the model, the direct incorporation of the vasculature and the relatively short diffusion length of oxygen (which is on the order of the diameter of five to six glial cells) does not allow the use of automaton cells which represent more than 50 cells, and a variable density lattice is not used. Finally, the original algorithm modeled neoplastic growth through the time of tumor-induced death while the current algorithm only models the early stages of glioma growth. Microscopic changes that occur in the later stages of tumor development, including genetic mutations, chromosomal aberrations and single-cell invasion would need to be incorporated for the model to span early and late tumor growth.

In an effort to study the complex interplay between the microenvironment and tumor growth, the aforementioned model is modified to explicitly account for the

microvasculature and how it evolves in space and time. To achieve this goal, we present a novel method for generating the vasculature of healthy brain tissue. A microscopic tumor is introduced into the brain, and as the neoplasm grows, it co-opts the existing brain vasculature. Compounds produced by the tumor interact with compounds produced by the vasculature via reaction–diffusion equations, and the concentration of key proteins (particularly, VEGF and the angiopoietins) mediate the processes of vessel regression and growth. This constantly evolving vasculature determines whether a tumor cell is well-oxygenated and able to divide (proliferative), insufficiently oxygenated and in G_0 arrest (non-proliferative/hypoxic) or necrotic. The simulation allows us to study the growth of a primary neoplasm from a small mass of cells to a macroscopic tumor mass. Furthermore, we are able to simulate how mutations that affect the angiogenic response subsequently affect tumor development.

2. Simulation procedure

The algorithm presented here can be broken into four parts: automaton cell generation, vasculature development, vasculature evolution and the proliferation routine in which individual tumor cells divide and evolve.

2.1. Automaton cell generation

The first step of the simulation is to generate the automaton cells. The underlying lattice for our algorithm is the Delaunay triangulation, which is the dual lattice of the Voronoi tessellation (Kansal et al., 2000a; Torquato, 2002). In order to develop the automaton cells, a prescribed number of random points are generated in the unit square using the process of random sequential addition (RSA) of hard circular disks (Kansal et al., 2000a; Torquato, 2002). In the RSA procedure, as a random point is generated, it is checked if the point falls within some fixed distance from any other point already placed in the system (Kansal et al., 2000a; Torquato, 2002). Points that fall too close to any other point are rejected, and all others are added to the system. Each cell in the final Voronoi lattice will contain exactly one of these accepted sites. The Voronoi cell is defined by the region of space nearer to a particular site than any other site. In two dimensions, this results in a collection of polygons that fill the plane (Kansal et al., 2000a; Torquato, 2002). In order to create the Voronoi tessellation of space, the list of random points created by the RSA process is fed to a program based on the sweep-line Voronoi algorithm developed by Fortune (1987). Each automaton cell created by this process is chosen to represent seven glial cells, a number that is small enough to give an average cell diameter less than the diffusion length of oxygen. While we could choose a number less than seven, this would significantly increase the computational time of the algorithm.

2.2. Development of the microvascular network

Once the automaton cells have been created, the microvasculature of the healthy brain must be generated. Normal capillaries are commonly represented using the Krogh cylinder model. In this model, the capillaries are assumed to be straight, parallel vessels with uniform spacing (Baish et al., 1996; Secomb et al., 2000). However, images of the cerebral microvasculature (Secomb et al., 2000) show that the assumption of regularly spaced, parallel capillaries is a poor approximation of the brain's capillary network. We propose a random analog of the Krogh cylinder model to generate a more physiologically relevant brain microvasculature. The capillary network is allowed to exist on a triangular lattice, which is overlaid on top of the unit square containing the automaton cells. In order to generate a blood vessel, a random site on the triangular lattice is chosen, as is the angle at which the vessel extends along the lattice. The vessel created is accepted as part of the vasculature and extends from its point of origin until the tissue boundary, provided that it does not violate any of the following three constraints:

1. The vessel cannot penetrate a cylinder of radius one lattice unit about an existing vessel oriented at the same angle (Fig. 1a).
2. The vessel cannot cause the intersection of three vessels at one lattice site (Fig. 1b).
3. The vessel must vascularize at least one unvascularized automaton cell (Fig. 1c).

If constraint 2 is violated, a truncated vessel that extends only from the point of origin until the intersection of another vessel in the system is created. If a vessel does not violate any of these constraints (Fig. 1d), the full-length vessel is added to the network. Constraints 1 and 3 are based on the observation that the vasculature of healthy tissue is optimally designed; that is, the minimum number of vessels supply the maximum number of cells with oxygen and nutrients. Constraint 2 is imposed because biological vessels are observed to branch from one vessel into two, but not from one vessel into three. The cells that are vascularized by each vessel placed in the tissue are determined. Vessels are laid down until each cell in the brain tissue under consideration is vascularized. This random analog of the Krogh cylinder model allows for the generation of more complex, tortuous vessels without making the oversimplifying assumption employed by others (Alarcón et al., 2005) that the vascular network obeys a simple ordered geometric pattern.

2.3. Vasculature evolution

Having established both the cell population and the capillary network, we can begin to consider the complex feedback that occurs between the growing tumor and the

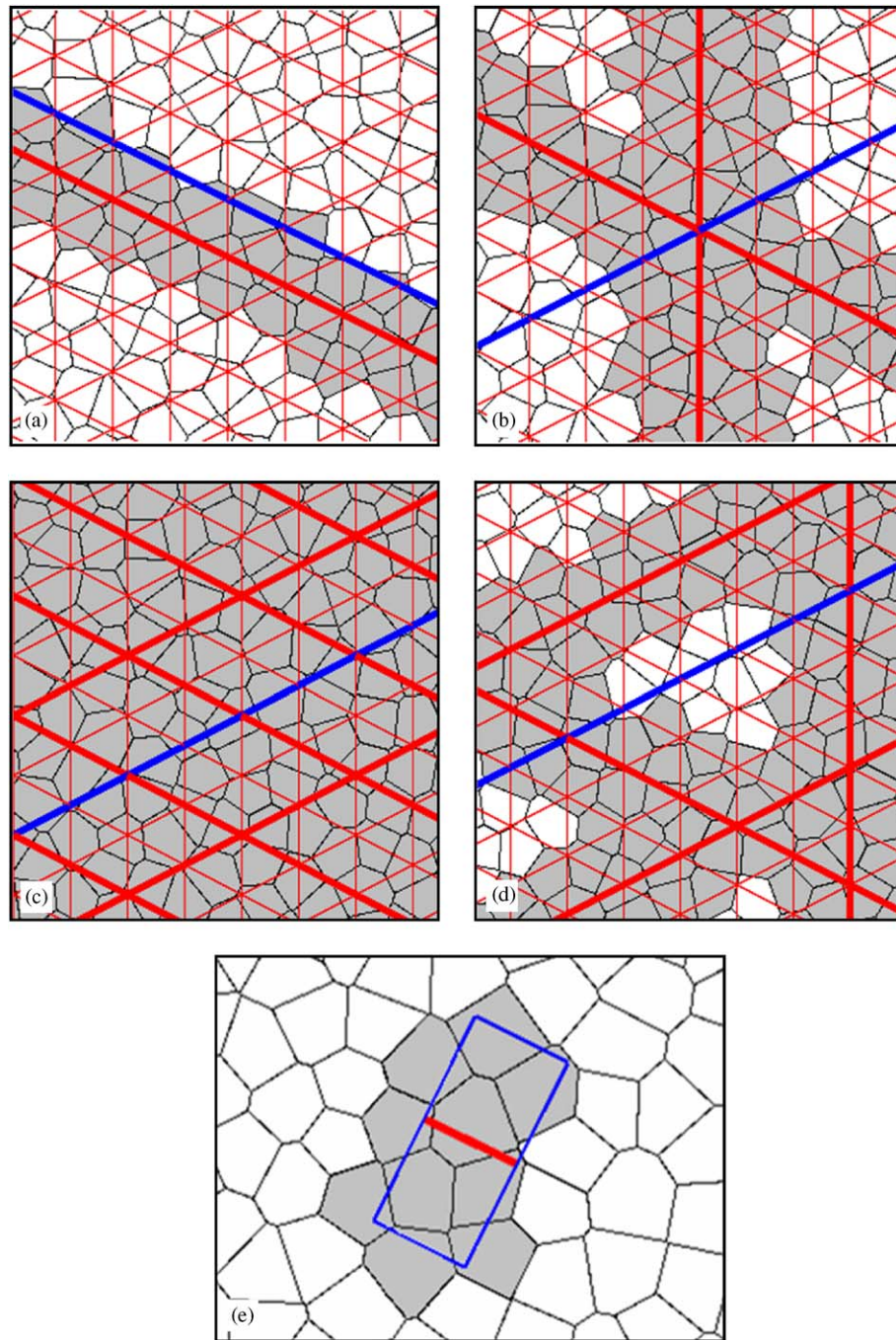


Fig. 1. Rules used in vasculature generation. Thin red lines denote pathways along which a vessel can be placed, thick red lines denote vessels already in the vasculature and thick blue lines denote the vessel that we are attempting to insert in the network. White cells are not vascularized by any vessel, and gray cells are vascularized by a vessel already in the system. (a) Reject the blue test vessel because it is too close to the vessel already in the system. (b) Reject the blue test vessel because it causes the intersection of three vessels at one lattice site. (c) Reject the blue test vessel since it vascularizes no unvascularized cells. (d) Accept the blue test vessel since it violates none of the constraints. (e) Determining which cells are vascularized by a blood vessel edge (thick red line).

brain microvasculature. To this end, we have developed a system of reaction–diffusion equations that predicts the evolution of key proteins and receptors that are involved in the processes of vessel regression and sprouting. Understanding the trajectories of these key angiogenic players will allow us to determine how each vessel in the

system evolves and, in turn, the evolution of individual automaton cells. The quantities that govern vasculature evolution are concentrations of VEGF (v), unbound VEGFR-2 (r_{v0}), VEGFR-2 bound by VEGF (r_v), Ang-1 (a_1), Ang-2 (a_2), the unbound angiopoietin receptor Tie-2 (r_{a0}), Tie-2 bound by Ang-1 (r_{a1}) and Tie-2 bound

by Ang-2 (r_{a2}). The model is developed under the following assumptions:

- Hypoxic tumor cells produce VEGF at a rate limited by the amount of VEGF at the site of the hypoxic cell (Tse et al., 2003). VEGF diffuses throughout the tissue, establishing a chemotactic gradient to which ECs can respond (Plank et al., 2004). VEGF can bind to the unoccupied VEGFR-2 and VEGF decays at a constant rate.
- Ang-2 is present in areas of vascular remodeling (i.e. produced by ECs associated with malignant tissue) and is hypoxia-inducible (i.e. produced by hypoxic cells). We have used the assumption that vessels associated with tumor tissue are undergoing vascular remodeling. The rate of Ang-2 production at a particular tissue site is modulated by the amount of Ang-2 at the site (Tse et al., 2003). Ang-2 can bind to EC-specific unoccupied Tie-2 receptors and Ang-2 decays at a constant rate.
- Ang-1 is constitutively expressed by ECs of healthy tissue (Holash et al., 1999a,b). In the absence of vascular remodeling, Ang-2 is absent from the system, and we assume that all Ang-1 is initially bound to a Tie-2 receptor.
- In tumor-associated vessels, Ang-1 production is limited by the concentration of Ang-1 at each site. Ang-1 is thought to act in a paracrine manner, so the diffusion of Ang-1 is neglected (Plank et al., 2004). Ang-1 competes with Ang-2 for Tie-2 binding, and Ang-1 decays at a constant rate.
- It has been shown that while VEGFR-2 is expressed on tumor endothelium (Brekken and Thorpe, 2001; Plate et al., 1993), VEGFR-2 is not expressed by ECs of the normal adult brain (Plate et al., 1993). For this reason, we assume that before a neoplasm is introduced in the system, VEGFR-2 is not expressed by any of the normal tissue ECs. Once a vessel becomes associated with tumor tissue, we assume for simplicities sake that VEGFR-2 is expressed at a constant level.
- It has been shown that there is no significant change in the expression of Tie-2 as the tumor grows, although the expression of Tie-2 is more noticeable at the tumor periphery (Tse et al., 2003). For simplicities sake, we assume that Tie-2 upregulation is negligible in both space and time, and we impose a constant level of Tie-2 expression throughout healthy and tumor-associated ECs.
- Since we have taken a discrete approach to modeling the vasculature, we chose not to introduce a continuum equation for EC density. Instead, we assume that if a blood vessel is present at a lattice site, the concentration of ECs at the site is constant. While it may seem that this assumption ignores the importance of EC proliferation induced by VEGF, we implicitly account for EC proliferation in the sprouting process.

Given these assumptions, the complete set of dynamic equations describing the interaction of VEGF, the angiopoietins and their respective receptors is

$$\frac{\partial v}{\partial t} = \underbrace{D_v \Delta v}_{\text{diffusion}} + \underbrace{b_v h_i (h - v^2 / K_v)}_{\text{production}} - \underbrace{k_0 v r_{v0}}_{\text{complex formation}} + \underbrace{k_{-0} r_v}_{\text{breakdown}} - \underbrace{\mu_v v}_{\text{decay}}, \quad (1)$$

$$\frac{\partial a_1}{\partial t} = \underbrace{b_{a1} e_i (p_i + h_i + n_i) (e_0 - a_1^2 / K_a)}_{\text{production}} - \underbrace{k_1 a_1 r_{a0}}_{\text{complex formation}} + \underbrace{k_{-1} r_{a1}}_{\text{breakdown}} - \underbrace{\mu_{a1} a_1}_{\text{decay}}, \quad (2)$$

$$\frac{\partial a_2}{\partial t} = \underbrace{D_{a2} \Delta a_2}_{\text{diffusion}} + \underbrace{b_{a2} e_i (p_i + h_i + n_i) (e_0 - a_2^2 / K_a)}_{\text{production}} + \underbrace{\bar{b}_{a2} h_i (h - a_2^2 / K_a)}_{\text{production}} - \underbrace{k_2 a_2 r_{a0}}_{\text{complex formation}} + \underbrace{k_{-2} r_{a2}}_{\text{breakdown}} - \underbrace{\mu_{a2} a_2}_{\text{decay}}, \quad (3)$$

$$\frac{\partial r_{v0}}{\partial t} = \underbrace{-k_0 v r_{v0}}_{\text{complex formation}} + \underbrace{k_{-0} r_v}_{\text{breakdown}}, \quad (4)$$

$$\frac{\partial r_{a0}}{\partial t} = \underbrace{-k_1 a_1 r_{a0}}_{\text{complex formation}} + \underbrace{k_{-1} r_{a1}}_{\text{breakdown}} - \underbrace{k_2 a_2 r_{a0}}_{\text{complex formation}} + \underbrace{k_{-2} r_{a2}}_{\text{breakdown}}, \quad (5)$$

$$\frac{\partial r_v}{\partial t} = \underbrace{k_0 v r_{v0}}_{\text{complex formation}} - \underbrace{k_{-0} r_v}_{\text{breakdown}}, \quad (6)$$

$$\frac{\partial r_{a1}}{\partial t} = \underbrace{k_1 a_1 r_{a0}}_{\text{complex formation}} - \underbrace{k_{-1} r_{a1}}_{\text{breakdown}}, \quad (7)$$

$$\frac{\partial r_{a2}}{\partial t} = \underbrace{k_2 a_2 r_{a0}}_{\text{complex formation}} - \underbrace{k_{-2} r_{a2}}_{\text{breakdown}}, \quad (8)$$

where each variable w_i represents a cell indicator function:

$$w_i(x, y, t) = \begin{cases} 1 & \text{if cell satisfies property } w, \\ 0 & \text{otherwise} \end{cases}$$

and

$$h(x, y, t) = \begin{cases} h_0 & \text{if cell is hypoxic,} \\ 0 & \text{otherwise.} \end{cases}$$

The complete list of variable definitions is found in Table 1 and the complete list of parameter definitions (along with the values used in the simulation) is found in Table 2.

Initially, there is no VEGF, VEGFR-2, free Ang-1 or Ang-2 or Tie-2 bound by Ang-2 in the system, so the initial

conditions for these variables are taken to be zero:

$$v(x, y, 0) = 0, \quad a_1(x, y, 0) = 0, \quad a_2(x, y, 0) = 0, \\ r_{v0}(x, y, 0) = 0, \quad r_v(x, y, 0) = 0, \quad r_{a2}(x, y, 0) = 0.$$

We assume that all ECs initially express unbound Tie-2 in the following manner:

$$r_{a0}(x, y, 0) = \begin{cases} \alpha - a_0 & \text{if part of a blood vessel,} \\ 0 & \text{otherwise.} \end{cases}$$

Table 1

Summary of variables in the system of reaction–diffusion equations given in (1)–(8)

Variable	Definition
$v(x, y, t)$	Concentration of VEGF (μM)
$a_1(x, y, t)$	Concentration of Ang-1 (μM)
$a_2(x, y, t)$	Concentration of Ang-2 (μM)
$r_{v0}(x, y, t)$	Concentration of unbound VEGFR-2 (μM)
$r_{a0}(x, y, t)$	Concentration of unbound Tie-2 (μM)
$r_v(x, y, t)$	Concentration of VEGFR-2 bound by VEGF (μM)
$r_{a1}(x, y, t)$	Concentration of Tie-2 bound by Ang-1 (μM)
$r_{a2}(x, y, t)$	Concentration of Tie-2 bound by Ang-2 (μM)
$e_i(x, y, t)$	EC indicator function
$h_i(x, y, t)$	Hypoxic cell indicator function
$p_i(x, y, t)$	Proliferative cell indicator function
$n_i(x, y, t)$	Necrotic cell indicator function
$h(x, y, t)$	Concentration of hypoxic cells (μM)

Table 2

Parameter definitions and the values used to numerically solve PDEs

Parameter definition	Value	Reference
Diffusion coefficient of VEGF	$D_v = 3.6 \times 10^{-4} \text{ mm}^2/\text{h}$	Anderson and Chaplain (1998)
Diffusion coefficient of Ang-2	$D_{a2} = 3.6 \times 10^{-4} \text{ mm}^2/\text{h}$	(–)
Production rate of VEGF by hypoxic cells	$b_v = 0.05 \text{ h}^{-1}$	(–)
Production rate of Ang-1 by ECs	$b_{a1} = 0.01 \text{ h}^{-1}$	(–)
Production rate of Ang-2 by ECs	$b_{a2} = 0.08 \text{ h}^{-1}$	(–)
Production rate of Ang-2 by hypoxic cells	$\tilde{b}_{a2} = 0.05 \text{ h}^{-1}$	(–)
Decay rate of VEGF	$\mu_v = 0.001 \text{ h}^{-1}$	(–)
Decay rate of Ang-1	$\mu_{a1} = 0.003 \text{ h}^{-1}$	(–)
Decay rate of Ang-2	$\mu_{a2} = 0.002 \text{ h}^{-1}$	(–)
Association rate of VEGF/VEGFR-2	$k_0 = 46.8/\mu\text{M h}$	Baldwin et al. (2001)
Dissociation rate of VEGF/VEGFR-2	$k_{-0} = 0.2268 \text{ h}^{-1}$	Baldwin et al. (2001)
Association rate of Ang-1/Tie-2	$k_1 = 36/\mu\text{M h}$	Longstaff (2002)
		Davis et al. (1996)
Dissociation rate of Ang-1/Tie-2	$k_{-1} = 0.1332 \text{ h}^{-1}$	Longstaff (2002)
		Davis et al. (1996)
Association rate of Ang-2/Tie-2	$k_2 = 41.7/\mu\text{M h}$	Maisonpierre et al. (1997)
		Longstaff (2002)
Dissociation rate of Ang-2/Tie-2	$k_{-2} = 0.108 \text{ h}^{-1}$	Maisonpierre et al. (1997)
		Longstaff (2002)
Initial concentration of Ang-1/Tie-2	$a_0 = 5 \times 10^{-6} \mu\text{M}$	(–)
Unbound receptor concentration	$\alpha = 10^{-4} \mu\text{M}^a$	Longstaff (2002)
EC concentration at each blood vessel	$e_0 = 10^{-4} \mu\text{M}$	Plank et al. (2004)
Cellular concentration at each vertex	$h_0 = 10^{-3} \mu\text{M}$	(–)
Carrying capacity of VEGF	$K_v = 10^{-2} \mu\text{M}$	(–)
Carrying capacity of angiopoietins	$K_a = 1.5 \times 10^{-2} \mu\text{M}$	(–)

Any reference given by (–) denotes that we have estimated the parameter value.

^aTypical values of receptor concentration can range anywhere from 10^{-4} to $10 \mu\text{M}$. The values used here do not represent physical values for these receptors, but instead represent one value in the typical range of receptor concentrations.

Finally, since there is a constitutive low-level expression of Ang-1 by ECs in healthy tissue, we take

$$r_{a1}(x, y, 0) = \begin{cases} a_0 & \text{if part of a blood vessel,} \\ 0 & \text{otherwise.} \end{cases}$$

Dirichlet boundary conditions are imposed at the boundary of the unit square, $\partial\Omega$:

$$v(\partial\Omega, t) = 0, \quad a_1(\partial\Omega, t) = 0, \quad a_2(\partial\Omega, t) = 0, \\ r_{v0}(\partial\Omega, t) = 0, \quad r_v(\partial\Omega, t) = 0, \quad r_{a2}(\partial\Omega, t) = 0,$$

$$r_{a0}(\partial\Omega, t) = \begin{cases} \alpha - a_0 & \text{if part of a blood vessel,} \\ 0 & \text{otherwise,} \end{cases}$$

$$r_{a1}(\partial\Omega, t) = \begin{cases} a_0 & \text{if part of a blood vessel,} \\ 0 & \text{otherwise.} \end{cases}$$

Whenever possible, parameter values have been taken from experimental data (see Table 2). Parameters that we were unable to find in the literature have been estimated.

Before proceeding with the discussion of the remainder of the algorithm, it is instructive to comment on the use of partial differential equations (PDEs) in the model. In most models of biological systems that involve differential equations, the goal is to make predictions on, for example, the time evolution and spatial distribution of chemical

concentrations. While this goal is important in its own right and has been undertaken by many in the field of angiogenesis modeling (Anderson and Chaplain, 1998; Hahnfeldt et al., 1999; Plank et al., 2004), this is not the goal of our modeling project. Instead, we are concerned with how the *relative* levels of different chemical species drive tumor growth. For example, experimental data has shown that a blood vessel will regress in the absence of VEGF if the level of bound Ang-2 is greater than six times the level of bound Ang-1 (Maisonpierre et al., 1997). Since the model is only concerned with the level of Ang-2 relative to Ang-1, the parameters which govern Ang-1 and Ang-2 production will only need to be known relative to one another, greatly reducing the number of effective parameters in the model and the need for absolute parameter values. In other words, we insist that our model only needs to capture the *relative* parameter values in order to be predictive.

A finite difference approximation on a triangular grid is used to numerically solve the system given by Eqs. (1)–(8) subject to the prescribed initial and boundary conditions. At each step of the algorithm, the concentration of bound VEGF relative to a threshold concentration and the ratio of the concentration of bound Ang-2 to bound Ang-1 is used to determine how the vasculature evolves at each lattice vertex. Particularly, if the concentration of Ang-2 satisfies the relation

$$r_{a2}(x,y,t) \geq a_{crit} \times r_{a1}(x,y,t),$$

and if the level of bound VEGF at the EC is below its critical value, rv_{crit} , we assume the vessel is unstable and regression of the vessel through its tip occurs. Any vessel tip that has a sufficient amount of bound VEGF (determined by the rv_{crit} parameter) is allowed to sprout. The vessel sprouts in the direction of greatest VEGF concentration. If there are multiple directions that have a level of VEGF greater than the VEGF concentration at the site under consideration, the vessel has a 50% chance of branching; i.e. sprouting in two directions.

Thus far, we have discussed the rules that allow a blood vessel to regress or sprout, but we have not accounted for the motility of the ECs nor have we considered the degradation of the extracellular matrix (ECM), a process that must occur for ECs to exit from pre-existing blood vessels. While a detailed mathematical description of the movement of ECs via diffusion, chemotaxis and haptotaxis

and the degradation of the ECM has been developed by others (Anderson and Chaplain, 1998; McDougall et al., 2006), we chose not to take such a detailed approach to model the movement of ECs. Instead, in order to account for EC motility, vessel tips that do not satisfy the sprouting requirements, but are at a location with sufficient levels of unbound VEGF, can potentially sprout in the direction of the VEGF gradient. This addition to the model allows us to account for the effects of EC motility towards areas of high VEGF concentration without explicitly incorporating such processes into the model.

2.4. Proliferation algorithm

Once the vasculature has established itself at a given time, the proliferation algorithm can be run. The simulation classifies automaton cells into one of the five types. There are two kinds of non-tumorous/healthy cells: viable cells that do not actively divide and apoptotic cells. There are three malignant cell types: proliferative cells that are well-vascularized and actively dividing, non-proliferative/hypoxic cells whose oxygen supply is insufficient to support cellular division and necrotic cells. With the exception of the apoptotic cells, all five cell types were present in the original versions of the model (Kansal et al., 2000a,b; Schmitz et al., 2002). The addition of blood vessels into the model necessitated the incorporation of non-malignant apoptotic cells, as explained in more detail below. An automaton cell is thus classified by its type (non-malignant or malignant) and its oxygen levels. The ideal way to determine the oxygen level of a cell would be to directly simulate blood flow through the capillary network (Alarcón et al., 2005; McDougall et al., 2002, 2006; Secomb et al., 2000). However, in an attempt to reduce the computational time of the algorithm, the following criteria is used to determine if an automaton cell is well-vascularized:

- For each edge on the triangular lattice that holds a blood vessel, a rectangle with a length that is two times the diffusion length of oxygen (l_{prolif}) and a width equal to the length of the vessel edge is drawn. Two sides of the rectangle run parallel to the edge, and the other two run perpendicular to the edge (Fig. 1e; Table 3).
- If an automaton cell falls within this rectangle, the cell is assumed to be vascularized.

Table 3
Parameter definitions and the values used in the proliferation algorithm (not used to solve PDEs)

Parameter definition	Value	Reference
Maximum diffusion length of oxygen	$l_{prolif} = 250 \mu\text{m}$	Zheng et al. (2005)
Maximum distance that tumor cell remains hypoxic	$l_{hyp} = 1500 \mu\text{m}$	(–)
Base probability of division	$p_0 = 0.192$	Kansal et al. (2000a)
Mechanical confinement parameter	$R_{max} = 10.0 \text{ mm}$	(–)
Critical ratio of bound Ang-2 to Ang-1	$a_{crit} = 6$	Maisonpierre et al. (1997)
Critical concentration of VEGF	$rv_{crit} = 4 \times 10^{-7} \mu\text{M}$	(–)

- If an automaton cell does not fall within this region for any vessel in the vasculature, the cell is not well-vascularized.

An intercellular mechanical stress (IMS) algorithm is used to accommodate cellular division (Kansal et al., 2000a). The IMS algorithm allows for the continuous division of all proliferative tumor cells, whether the cells are found at the tumor edge or not. Similar to the original algorithm, proliferative cells can transition to hypoxic cells and hypoxic cells can transition to necrotic cells (Kansal et al., 2000a). Unlike in the original model, hypoxic cells can transition to proliferative cells if the evolution of the vasculature sufficiently increases the oxygen supply of the cell. Further, blood vessel regression can cut off the blood supply of both cancerous and healthy cells. Unlike neoplastic cells, non malignant cells lack the ability to survive in oxygen and nutrient-deprived environments. Hence, when vessel regression cuts off the oxygen and nutrient supply of a healthy cell, we assume that this non malignant cell undergoes apoptosis.

We now consider the algorithm that is used to couple capillary network and tumor evolution. The first step is to lay down the vasculature and designate the center automaton cell as a proliferative cell. The remaining cells are declared to be non-tumorous. Time is then discretized into units that represent one real day. At each time step:

- The system of PDEs governing the dynamics of VEGF, the angiopoietins and their receptors is numerically solved one day forward in time.
- Each vessel is checked to see if it meets the requirements for regression. Any vessels meeting regression requirements are destroyed.
- Each vessel tip is checked to see if it meets the requirements to sprout and possibly to branch. Any vessel tip that satisfies the sprouting requirement grows in the direction of maximum VEGF concentration.
- Each cell is checked for type: non-tumorous (either viable or apoptotic), proliferative, non-proliferative/hypoxic or necrotic (Kansal et al., 2000a).
- Non-tumorous apoptotic cells neighboring healthy tissue are inert, unless the location of such a cell becomes well-oxygenated. If this occurs, the apoptotic cell is engulfed by phagocytes and its space is filled with a healthy cell.
- Non-tumorous apoptotic cells neighboring tumorous tissue are inert.
- Non-tumorous viable cells undergo apoptosis if their oxygen supply is cut off.
- Necrotic tumor cells are inert (Kansal et al., 2000a).
- Hypoxic cells that become well-oxygenated by the evolution of the vasculature are turned proliferative.
- Hypoxic cells that are located too far from a vessel to remain hypoxic (at a distance greater than l_{hyp} ; see Table 3) turn necrotic.
- Each well-oxygenated proliferative cell will attempt to divide into the space of a viable non-malignant cell. The probability of division, p_d , is influenced by the radial distance of the dividing cell (r). This reflects the effects of mechanical confinement pressure:

$$p_d = p_0(1 - r/R_{max}), \quad (9)$$
 where p_0 is the base probability of division (linked to cell doubling time) and R_{max} is the maximum tumor extent, controlled by the pressure response of the tumor to the confinements of the brain (Kansal et al., 2000a).
- Proliferative cells that are no longer well-oxygenated (at a distance greater than l_{prolif} ; see Table 3) are turned hypoxic.
- The tumor radius, R_t , is calculated after each automaton element has evolved. The radius is calculated by averaging over the radial distance (r_i) of each cell on the tumor edge:

$$R_t = \left(\sum_{i=1}^N r_i \right) / N, \quad (10)$$
 where there are N cells found on the tumor edge (Kansal et al., 2000a). The tumor area is also calculated at each time step.

In the current investigation, the unit square is divided into 26,483 automaton cells. Since a glial cell has an average diameter of 40 μm (Broaddus et al., 2004), by designating one automaton cell to represent seven glial cells, each automaton cell has an average diameter of 120 μm . Therefore, the unit square represents a 24 mm \times 24 mm region of brain tissue.

3. Results

We present our results in the following fashion. First, we discuss the features of the vasculature created via the random analog of the Krogh cylinder model. Second, we demonstrate the versatility of our model by studying tumor growth in two cases: when the tumor initiates angiogenesis, and when angiogenesis is not successfully induced.

Simulations were created using a tumor that was grown from an initial radius of 0.1 mm. The parameter set used to solve the PDEs can be found in Table 2. Additionally, six parameters (that were not needed to solve the PDEs) were used to govern the evolution of the vasculature and the individual tumor cells (Table 3). We note that the base probability of division, $p_0 = 0.192$, corresponds to a realistic glioma cell-doubling time of approximately four days (Kansal et al., 2000a). Furthermore, while we do not have a precise value for the VEGF threshold rv_{crit} , it is known that a certain threshold concentration of VEGF is required to inhibit EC apoptosis and to trigger angiogenesis (Neufeld et al., 1999).

In the visualizations of the tumor that follow, we use the following convention: viable non malignant cells are labeled

white, non malignant cells that have undergone apoptosis are green, necrotic tumor cells are black, non-proliferative/hypoxic tumor cells are yellow and proliferative tumor cells are blue. Further, in the visualization of the vasculature, we use the following convention: vessels that are originally part of the healthy brain capillary network are labeled red and vessels that grow via angiogenesis are labeled purple.

3.1. Microvascular network

The normal vascular microenvironment is typically ignored in models of tumor growth, despite the intimate connection between the healthy tissue vasculature and the tumor-associated vasculature. In order to couple the processes of vessel co-option, regression and angiogenesis to tumor growth, a realistic model of the normal microvascular network is required. Several different algorithms have been developed to deduce the geometry of the vascular network using SEM (Secomb et al., 2000) or intravital microscopy images of the brain (Hudetz et al., 1993). For our purposes, it is unnecessary to use a computationally expensive reconstruction procedure to describe the capillary network of the brain. Instead, using the random analog of the Krogh cylinder model presented in the Simulation Procedure section, we have produced a vascular network (Fig. 2) that does not reproduce an actual brain capillary network, but instead exhibits features that are typical of the brain's microvascular environment and is more physiologically relevant than the vasculature developed via the standard Krogh cylinder model.

One observation that has been made about the microvascular network of the brain is that capillary density and

network pattern varies from region to region (Hudetz et al., 1993). Our model captures this feature of the vasculature, as some areas of the tissue presented in Fig. 2 have a higher capillary density than others. Another characteristic of the brain capillary network is the irregular pattern of tortuous capillaries (Hudetz et al., 1993). While the Krogh cylinder model does not account for such irregular branching patterns, the random analog of the model results in a vasculature where branching numbers vary from vessel to vessel. Finally, it is believed that vessels in healthy tissue leave no cell farther from a vessel than the maximum diffusion distance of oxygen and nutrients (Baish et al., 1996). By developing the vasculature until all cells are within a fixed distance from a vessel, we are also capturing this feature of the brain microvasculature.

3.2. Tumor evolution with angiogenesis

Figure 3 shows the evolution of the vascular network and the tumor in the case where the VEGFR-2 pathway is sufficiently stimulated. The tumor begins as a small mass of proliferative cells. The production of Ang-2 by the tumor-associated capillaries leads to frank vessel regression and the production of hypoxic regions within the tumor (Fig. 3a). We also observe that a handful of healthy cells surrounding the growing tumor have undergone apoptosis as a result of blood vessel regression. Tumor-cell hypoxia then triggers the production of VEGF. As VEGF diffuses throughout the tissue, it establishes a concentration gradient to which ECs are chemoattracted. The ECs begin to move on this VEGF gradient, and the binding of VEGF to VEGFR-2 triggers EC sprouting. The angiogenic vessels created via capillary sprouting penetrate the tumor (Fig. 3b), rescuing what would otherwise become a hypoxic/necrotic mass of cells.

It has been observed that the growth of vessels via angiogenesis does not occur in the same orderly fashion as the formation of the healthy vascular network. The network that forms during normal development is driven by a global response to a physiological stimulus such as oxygen delivery, whereas the network that forms via angiogenesis is driven by local heterogeneity in the tumor, such as VEGF concentration (Baish et al., 1996). The fact that angiogenic capillaries sprout in response to the local environment is consistent with the observation that the angiogenic vascular network has a chaotic, fractal appearance (Baish et al., 1996). The chaotic appearance of the tumor-associated vasculature is captured in our simulation (Fig. 3c,d). We observe that the angiogenic capillaries that penetrate the tumor are found in dense clusters, have a much higher branching number than the vessels associated with the healthy vasculature and contain many tortuous vessels. All of these observations are consistent with the fractal nature of tumor-associated vessels generated via angiogenesis (Baish et al., 1996).

The radius and area of the two-dimensional developing tumor are shown versus time in Fig. 4. Recall that we can

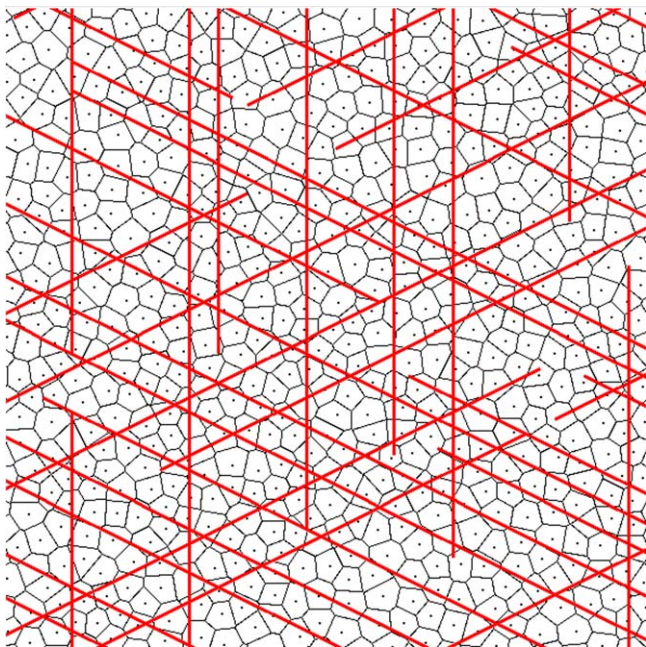


Fig. 2. A portion of the microvascular network of normal brain tissue developed using the random analog of the Krogh cylinder model.

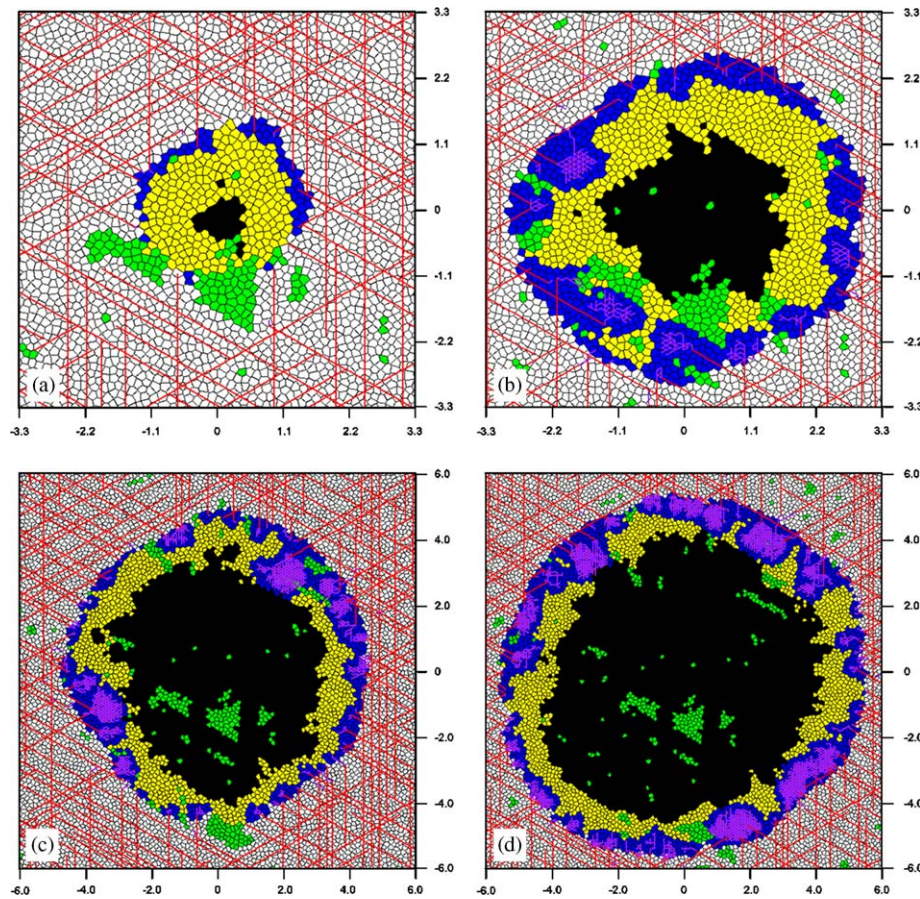


Fig. 3. The temporal development of a cross-central section of a tumor in the presence of properly functioning angiogenic mechanisms. (a) Radius of tumor at day 40 is 1.58 mm. (b) Radius of tumor at day 70 is 3.09 mm. (c) Radius of tumor at day 100 is 4.53 mm. (d) Radius of tumor at day 130 is 5.84 mm. The blue outer region is comprised of proliferative cells, the yellow region consists of hypoxic cells and the black center contains necrotic cells. Green cells are apoptotic. The scales are in millimeters.

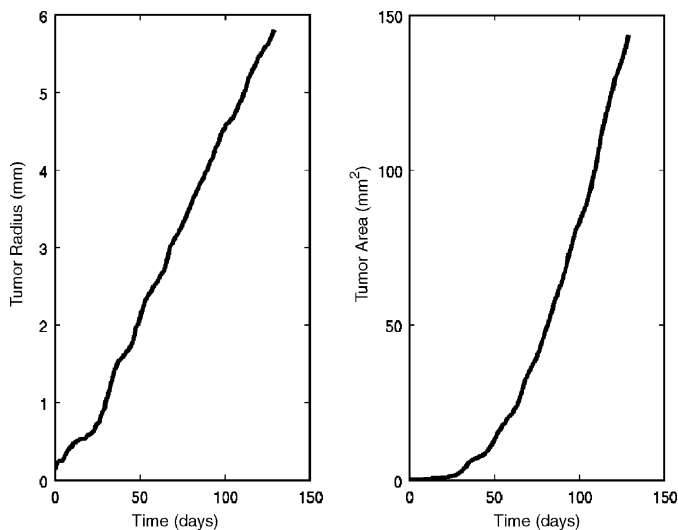


Fig. 4. Tumor radius and area as a function of time.

think of these growth curves as representing the growth of a cross-central slice of a three-dimensional tumor mass. Summarized in Table 4 is the comparison between the new simulation results, the old simulation results and data

Table 4

Comparison of the growth fraction (percent of proliferative cells) for a test case and simulation results (both from the original algorithm and the new algorithm) at fixed tumor radii

	Time	Radius (mm)	Growth fraction (%)
New algorithm: 2D	Day 17	0.53	35
New algorithm: 2D	Day 111	4.96	31
Old algorithm: 3D	Day 69	0.5	35
Old algorithm: 3D	Day 223	5.0	30
Data	—	0.5	36
Data	—	5.0	30

Note that the time column is simulation data only and is taken from the start of the simulation, not from the theoretical start of tumor growth.

(both clinical and experimental) (Kansal et al., 2000a). The growth fraction of the tumor at fixed radii as predicted by the old and new model is in good agreement with experimental data. We note that the time difference observed for achieving the same radius in the old and new model is a result of the dimension in which the tumor is growing: radial growth occurs faster in two dimensions than in three dimensions.

3.3. Tumor evolution without angiogenesis

We can now focus on tumor evolution when angiogenesis is unsuccessfully induced by a growing tumor. In particular, this section will simulate tumor growth under one of the following scenarios: VEGF is not secreted by hypoxic tumor cells due to a mutation in the HIF-1 pathway (Brat et al., 2003), VEGF is mutated, VEGFR-2 is mutated or inhibited or there is a mutation in a key player of the VEGF-VEGFR-2 pathway, and the binding of VEGF to VEGFR-2 does not trigger the usual angiogenic responses, including EC proliferation and the prevention of EC apoptosis.

Fig. 5 shows how both the vascular network and tumor evolve in the absence of angiogenesis. The tumor begins as a small mass of proliferative cells that have co-opted the vasculature of its host environment. The ECs associated with the tumor co-opted vessels begin to produce Ang-2, and the ratio between bound Ang-2 and bound Ang-1 shifts in favor of Ang-2. In the absence of functional VEGF, this destabilizes the tumor-associated capillaries, and vessel regression is observed (Fig. 5a,b). Since the nutrients and oxygen required to maintain active growth are no longer reaching the cancerous cells, hypoxic regions begin to overwhelm the tumor (Fig. 5b,c). We also observe

that a number of healthy cells have undergone apoptosis as a result of vessel regression.

In the absence of a compensatory angiogenic response, the continuing loss of tumor-associated blood vessels results in an avascular, hypoxic tumor mass (Fig. 5d). This final tumor has a diameter of approximately 1.4 mm, which is consistent with the experimental observation that, without the formation of new blood vessels, solid tumors can grow no larger than 1–2 mm in diameter (Brat et al., 2003).

4. Discussion

The macroscopic properties of a neoplastic mass are determined by multiple intracellular feedback loops within individual tumor cells, and by complex, multidirectional interaction loops that occur between tumor cells and the stroma, ECM, immune cells, the vasculature and other tumor cells (Kitano, 2004). In an effort to understand tumor dynamics, it is essential to elucidate these poorly understood interactions that occur between the tumor and the host microenvironment (Kitano, 2004). As a first step towards achieving this goal, we have developed a two-dimensional hybrid cellular automaton model (extended from a previously designed proliferation algorithm)

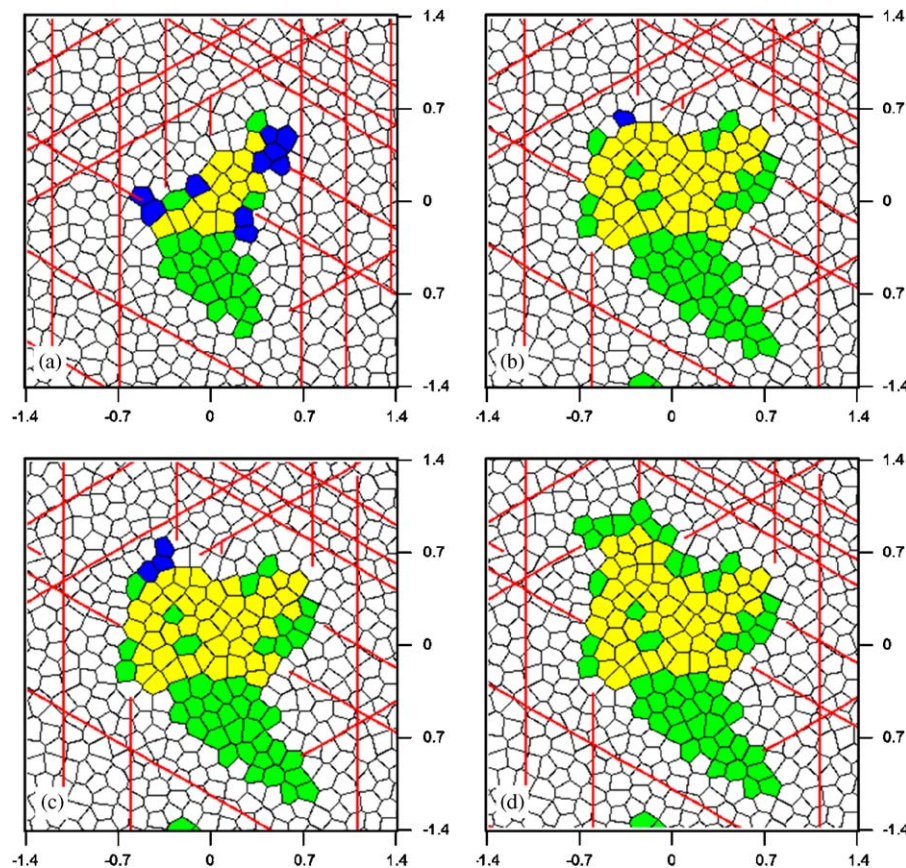


Fig. 5. The temporal development of a cross-central section of a tumor growing without angiogenesis. (a) Radius of tumor at day 20 is 0.56 mm. (b) Radius of tumor at day 40 is 0.69 mm. (c) Radius of tumor at day 60 is 0.70 mm. (d) Radius of tumor at day 80 is 0.72 mm. The scales are in millimeters.

examining the feedback that occurs between the host/tumor microvasculature and the individual tumor cells at early stages of neoplastic growth. To our knowledge, this is the first computational model of solid tumor growth that couples the evolution of the microvasculature (both vessel regression and sprouting) with the evolution of the tumor mass.

Our computational model assumes that the main regulators of glioma angiogenesis are vascular endothelial growth factor and the angiopoietins. Our simulations predict that if Ang-2 is significantly upregulated relative to Ang-1, and if the VEGF-VEGFR-2 pathway is stimulated under hypoxic conditions, angiogenesis is induced and a microscopic tumor mass can grow to a macroscopic size (Fig. 3). However, if this pathway is not properly stimulated, angiogenesis does not occur and a tumor mass cannot grow beyond a microscopic size of 1–2 mm in diameter (Fig. 5). In other words, our model supports Folkman's hypothesis that an "angiogenic switch" exists, and that VEGF and the angiopoietins are key players in this switch. Our model indicates that the tumor must overcome hypoxia and vessel regression in order to switch to the angiogenic phenotype.

The model highlights the very interesting role that Ang-2 plays in tumor growth in well-vascularized environments. Particularly, under the assumption that neoplasms growing in well-vascularized environments co-opt the host microvasculature, Ang-2 can be seen to act as both an anti-growth and a pro-growth signal for the tumor. If we envision a growing tumor as a self-organizing complex dynamic system (Kansal et al., 2000a), instead of as a random, disorganized mass of cells, it is interesting to consider why the tumor has evolved a system that actually leads to the destruction and recreation of its blood supply.

Most existing models of angiogenesis lead to the proposal of anti-angiogenic therapies (Alarcón et al., 2005; Hahnfeldt et al., 1999; Plank et al., 2004). However, what most of these models do is identify factors that will limit angiogenesis, not necessarily tumor growth. Our model has shown that if a tumor grows in a well-vascularized environment, as long as vessel regression does not occur, vessel co-option allows neoplastic growth to be sustained without angiogenesis. The idea that preventing angiogenesis may not limit tumor growth has therapeutic implications. To illustrate, we consider the commonly proposed anti-angiogenic therapy that aims at inhibiting Ang-2 (Holash et al., 1999a,b; Maisonpierre et al., 1997; Plank et al., 2004). Our model predicts that the inhibition of Ang-2 results in the survival of tumor-associated co-opted vessels, and while angiogenesis is inhibited, tumor growth can still occur (data not shown). It has also been suggested (Davis et al., 1996; Plank et al., 2004) that the exogenous administration of Ang-1 may impede angiogenesis, and hence limit tumor growth. Our model predicts that an increase in the level of Ang-1 stabilizes the existing vasculature, in turn limiting angiogenesis, but not tumor

growth (data not shown). Again, the co-option of the healthy vasculature by the tumor mass allows for the neoplasm to grow in the absence of angiogenesis.

As we move towards an understanding of the mechanisms that maintain a solid tumor, we can also begin to look for therapeutic approaches that target the weaknesses of the tumor system. In other words, we do not want to look for anti-angiogenic therapies that only impede angiogenesis, but therapies that can impede both angiogenesis and tumor expansion. As our model is the first to couple the changes in the microvasculature (both proliferative and regressive) with changes in the tumor, we are in a unique situation to find and exploit the weaknesses of the tumor–microvasculature system. For example, our results indicate that the administration of Ang-2 or the blocking of Tie-2 in combination with the inhibition of the VEGF-VEGFR-2 pathway will lead to vessel regression and the inhibition angiogenesis, hence thwarting further tumor growth. While these ideas have been proposed by others (Maher et al., 2001; Plank et al., 2004), to our knowledge our model is the first to show that these combinations of events will push a growing tumor into the zero growth-rate regime.

In summary, this work represents a first step at an attempt to elucidate the multiple, complex feedback loops that influence tumor development. While the feedback that occurs between the host microvasculature and the tumor is only one of many interactions that must be accounted for, it is also one of the most important ones. As we work to uncover how the multiple feedback loops maintain the tumor, we can begin to identify those loops that are detrimental to the host, and work to effectively inhibit/control these loops to thwart neoplastic growth.

Several directions are available to extend the present work. One obvious avenue is to incorporate more pro- and anti-angiogenic compounds into the model in order to assess the efficacy of many different therapeutic approaches. For example, other positive regulators of angiogenesis not considered in the current model, including basic fibroblast growth factor (bFGF), acidic fibroblast growth factor (aFGF), platelet-derived growth factor (PDGF), interleukin-8 (IL-8) and tumor necrosis factor alpha (TNF- α), have been identified (Folkman, 2003), as have many other negative regulators of angiogenesis, including angiostatin, endostatin and thrombospondin (Folkman, 2003). There are pluses and minuses to incorporating more proteins and receptors into the model. On the one hand, given the large number of players involved in angiogenesis, the incorporation of only three proteins and two receptors may be insufficient in analysing the angiogenic pathway. On the other hand, the inclusion of too many factors may overparameterize the system. Given that the biological parameters governing these proteins are mostly unknown, we currently choose to work with a minimal amount of angiogenic factors. Even with our simplistic model, there are several parameters that had

to be estimated, which is an undesirable but prominent feature of differential equation models.

A complete understanding of tumor–microvasculature interactions would require that we explicitly account for other aspects of angiogenesis in the model, including the degradation of the ECM, and the migration of the ECs via both chemotaxis along VEGF gradients and haptotaxis along fibronectin gradients of the ECM (Anderson and Chaplain, 1998; McDougall et al., 2006). While the current framework implicitly captures these features, the addition of such processes would improve the microscopic detail of the model. Another aspect that is absent in our model is blood flow through the capillary network. We make the simplifying assumption that any cell within a fixed distance from a vessel is well-oxygenated, which is not necessarily the case. Vessel diameter and tortuosity are both known to affect the diffusion length of oxygen and nutrients (Baish et al., 1996; Secomb et al., 2000). Blood flow has been incorporated in many other models of angiogenesis (Alarcón et al., 2005; McDougall et al., 2002, 2006; Secomb et al., 2000).

Angiogenesis is just one of the many key processes that govern tumor dynamics. Another step on our way to developing a comprehensive multiscale model of glioma growth is to incorporate other important features of gliomas, including specific genetic mutations and single-cell invasion. One key feature of tumor cells is uncontrolled growth. As a result of unchecked growth, tumor cells carrying mutations are generally not thwarted at cell cycle checkpoints, and mutations are able to accumulate. In future work, we hope to study the effects that mutations in tumor suppressor genes and oncogenes have on glioma dynamics. By differentiating between the behavior of cells with different clonal origins, a heterogeneous tumor with multiple competing strains will begin to develop. Growth patterns will be largely dependent on the mutations that are most beneficial to the tumor, and we can analyze how neoplastic growth and treatment strategies are influenced by the emergence of diverse clonal populations (Kansal et al., 2000b).

Finally, tumor-cell invasion is a hallmark of gliomas (Giese and Manfred, 1996). Individual glioma cells have been observed to spread diffusely over long distances and can migrate into regions of the brain essential for the survival of the patient (Holland, 2000). While MRI scans can recognize mass tumor lesions, these scans are not sensitive enough to identify malignant cells that have spread well beyond the tumor margin (Visted et al., 2003). Typically, when a solid tumor is removed, these invasive cells are left behind and tumor recurrence is almost inevitable (Holland, 2000). We hope to extend the hybrid cellular automaton model in the future in order to address the impact that the tumor vasculature, cell–cell adhesion and long-range cell signaling (Kansal and Torquato, 2001) have on single-cell invasion and treatment. In particular, recent mathematical models (Cristini et al., 2005; Frieboes et al., 2006) have demonstrated that the invasive phenotype

of tumor cells is favored in the presence of a heterogeneous distribution of oxygen and nutrients, while suppressed in the presence of a homogeneous oxygen distribution. When a heterogeneous distribution of oxygen and nutrients results in rapidly proliferating areas within the tumor, instability in the form of invasive fingering is triggered (Cristini et al., 2005; Frieboes et al., 2006). If our hybrid cellular automaton model was reduced to the single-cell level, the observation that vascular heterogeneity encourages cell motility can be used to predict which tumor cells will develop the invasive phenotype. The movement of these invasive cells can be tracked along the blood vessels in the model, allowing us to study the distribution of these invasive cells along the heterogeneous vasculature.

Acknowledgments

The authors benefited from helpful discussion with David Zagzag. J.L.G. would like to thank Pavithra Shivakumar for her invaluable programming advice. This project was partially supported by the National Science Foundation's GRFP.

References

- Alarcón, T., Byrne, H.M., Maini, P.K., 2005. A multiple scale model for tumor growth. *Multiscale Model. Simul.* 3 (2), 440–475.
- Anderson, A.R.A., Chaplain, M.A.J., 1998. Continuous and discrete mathematical models of tumor-induced angiogenesis. *Bull. Math. Biol.* 60, 857–900.
- Baish, J.W., Gazit, Y., Berk, D.A., Nozue, M., Baxter, L.T., Jain, R.K., 1996. Role of tumor vascular architecture in nutrient and drug delivery: an invasion percolation-based network model. *Microvasc. Res.* 51, 327–346.
- Baldwin, M.E., Catimel, B., Nice, E.C., Roufai, S., Hall, N.E., Stenvers, K.L., Karkkainen, M.J., Alitalo, K., Stacker, S.A., Achen, M.G., 2001. The specificity of receptor binding by vascular endothelial growth factor-D is different in mouse and man. *J. Biol. Chem.* 276 (22), 19166–19171.
- Brat, D.J., Kaur, B., Van Meir, E.G., 2003. Genetic modulation of hypoxia induced gene expression and angiogenesis: relevance to brain tumors. *Front. Biosci.* 8, d100–d116.
- Brat, D.J., Castellano-Sanchez, A.A., Hunter, S.B., Pecot, M., Cohen, C., Hammond, E.H., Devi, S.N., Kaur, B., Van Meir, E.G., 2004. Pseudopalisades in glioblastoma are hypoxic, express extracellular matrix proteases, and are formed by an actively migrating cell population. *Cancer Res.* 64, 920–927.
- Brekken, R.A., Thorpe, P.E., 2001. VEGF–VEGF receptor complexes as markers of tumor vascular endothelium. *J. Controlled Release* 74, 173–181.
- Broadbent, W.C., Haar, P.J., Gillies, G.T., 2004. *Nanoscale neurosurgery*. Encyclopedia of Biomaterials and Biomedical Engineering. Marcel Dekker, Inc., New York, pp. 1035–1042.
- Cristini, V., Frieboes, H.B., Gatenby, R., Caerta, S., Ferrari, M., Sinek, J., 2005. Morphological instability and cancer invasion. *Clin. Cancer Res.* 11 (19), 6772–6779.
- Davis, S., Aldrich, T.H., Jones, P.F., Acheson, A., Compton, D.L., Vivek, J., Ryan, T.E., Bruno, J., Radziejewski, C., Maisonpierre, P.C., Yancopoulos, G.D., 1996. Isolation of angiopoietin-1, a ligand for the Tie2 receptor, by secretion-trap expression cloning. *Cell* 87, 1161–1169.
- Folkman, J., 2003. Fundamental concepts of the angiogenic process. *Curr. Mol. Med.* 3, 643–651.

- Fortune, S., 1987. Sweepline algorithms for Voronoi diagrams. *Algorithmica* 2, 153–174.
- Frieboes, H.B., Zheng, X., Sun, C.-H., Tromberg, B., Gatenby, R., Cristini, V., 2006. An integrated computational/experimental model of tumor invasion. *Cancer Res.* 66 (3), 1597–1604.
- Giese, A., Manfred, W., 1996. Glioma invasion in the central nervous system. *Neurosurgery* 39 (2), 235–252.
- Hahnfeldt, P., Panigrahy, D., Folkman, J., Hlatky, L., 1999. Tumor development under angiogenic signaling: a dynamical theory of tumor growth, treatment, response, and postvascular dormancy. *Cancer Res.* 59, 4770–4775.
- Hatzikirou, H., Duetsch, A., Schaller, C., Simon, M., Swanson, K., 2005. Mathematical modelling of glioblastoma tumour development: a review. *Math. Models Methods Appl. Sci.* 15 (11), 1779–1794.
- Holash, J., Maisonpierre, P.C., Compton, D., Boland, P., Alexander, C.R., Zagzag, D., Yancopoulos, G.D., Wiegand, S.J., 1999a. Vessel cooption, regression, and growth in tumors mediated by angiopoietins and VEGF. *Science* 284, 1994–1998.
- Holash, J., Wiegand, S.J., Yancopoulos, G.D., 1999b. New model of tumor angiogenesis: dynamic balance between vessel regression and growth mediated by angiopoietins and VEGF. *Oncogene* 18, 5356–5362.
- Holland, E.C., 2000. Glioblastoma multiforme: the terminator. *Proc. Natl Acad. Sci.* 97 (12), 6242–6244.
- Hudetz, A.G., Greene, A.S., Fehér, G., Knuese, D.E., Coley, A.W., 1993. Imaging system for three-dimensional mapping of cerebrocortical capillary networks in vivo. *Microvasc. Res.* 46, 293–309.
- Hullemann, E., Helin, K., 2005. Molecular mechanisms in gliomagenesis. *Adv. Cancer Res.* 94, 1–27.
- Kansal, A.R., Torquato, S., 2001. Globally and locally minimal weight spanning tree networks. *Physica A* 301, 601–619.
- Kansal, A.R., Torquato, S., Harsh, G.R., Chiocca, E.A., Deisboeck, T.S., 2000a. Simulated brain tumor growth dynamics using a three-dimensional cellular automaton. *J. Theor. Biol.* 203, 367–382.
- Kansal, A.R., Torquato, S., Chiocca, E.A., Deisboeck, T.S., 2000b. Emergence of a subpopulation in a computational model of tumor growth. *J. Theor. Biol.* 207, 431–441.
- Kitano, H., 2004. Cancer as a robust system: implications for anticancer therapy. *Nat. Rev. Cancer* 4, 227–235.
- Levine, H.A., Pamuk, S., Sleeman, B.D., Nilsen-Hamilton, M., 2001. Mathematical modeling of capillary formation and development in tumor angiogenesis: penetration into the stroma. *Bull. Math. Biol.* 63, 801–863.
- Longstaff, C., 2002. Plasminogen activation of the cell surface. *Front. Biosci.* 7, 244–255.
- Maher, E.A., Furnari, F.B., Bachoo, R.M., Rowitch, D.H., Louis, D.N., Cavenee, W.K., DePinho, R.A., 2001. Malignant glioma: genetics and biology of a grave matter. *Genes Dev.* 15, 1311–1333.
- Maisonpierre, C.S., Suri, C., Jones, P.F., Bartunkova, S., Wiegand, S.J., Radziejewski, C., Compton, D., McClain, J., Aldrich, T.H., Papadopoulos, N., Daly, T.J., Davis, S., Sato, T.N., Yancopoulos, G.D., 1997. Angiopoietin-2, a natural antagonist for Tie2 that disrupts in vivo angiogenesis. *Science* 277, 55–60.
- McDougall, S.R., Anderson, A.R.A., Chaplain, M.A.J., Sherratt, J.A., 2002. Mathematical modelling of flow through vascular networks: implications for tumor-induced angiogenesis and chemotherapy strategies. *Bull. Math. Biol.* 64, 673–702.
- McDougall, S.R., Anderson, A.R.A., Chaplain, M.A.J., 2006. Mathematical modelling of dynamic adaptive tumour-induced angiogenesis: clinical implications and therapeutic targeting strategies. *J. Theor. Biol.* 241, 564–589.
- Neufeld, G., Cohen, T., Gengrinovitch, S., Poltorak, Z., 1999. Vascular endothelial growth factor (VEGF) and its receptors. *FASEB* 13, 9–22.
- Plank, M.J., Sleeman, B.D., Jones, P.F., 2004. A mathematical model of tumour angiogenesis, regulated by vascular endothelial growth factor and the angiopoietins. *J. Theor. Biol.* 229, 435–454.
- Plate, K.H., Breier, G., Millauer, B., Ullrich, A., Risau, W., 1993. Up-regulation of vascular endothelial growth factor and its cognate receptors in a rat glioma model of tumor angiogenesis. *Cancer Res.* 53, 5822–5827.
- Scalerandi, M., Sansone, B.C., 2002. Inhibition of vascularization in tumor growth. *Phys. Rev. Lett.* 89 (21), 218101.
- Scalerandi, M., Sansone, B.C., Condat, C.A., 2001. Diffusion with evolving sources and competing sinks: development of angiogenesis. *Phys. Rev. E* 65 (1), 011902.
- Schmitz, J.E., Kansal, A.R., Torquato, S., 2002. A cellular automaton model of brain tumor treatment and resistance. *J. Theor. Med.* 4 (4), 223–239.
- Secomb, T.W., Hsu, R., Beamer, N.B., Coull, B.M., 2000. Theoretical simulation of oxygen transport to brain by networks of microvessels: effects on oxygen supply and demand on tissue hypoxia. *Microcirculation* 7, 237–247.
- Singh, S.K., Clarke, I.D., Hide, T., Dirks, P.B., 2004a. Cancer stem cells in nervous system tissues. *Oncogene* 23, 7267–7273.
- Singh, S.K., Hawkins, C., Clarke, I.D., Squire, J.A., Bayani, J., Hide, T., Mekelman, R.M., Cusimano, M.D., Dirks, P.B., 2004b. Identification of human brain tumour initiating cells. *Nature* 432, 396–401.
- Torquato, S., 2002. *Random Heterogeneous Materials: Microstructure and Macroscopic Properties*. Springer, New York.
- Tse, V., Xu, L., Yung, Y.C., Santarelli, J.G., Juan, D., Fabel, K., Silverberg, G., Harsh IV, G., 2003. The temporal-spatial expression of VEGF, angiopoietin-1 and 2, and Tie-2 during tumor angiogenesis and their functional correlation with tumor neovascular architecture. *Neurol. Res.* 25, 729–738.
- Visted, T., Enger, P.O., Lund-Johansen, M., Bjerkvig, R., 2003. Mechanisms of tumor cell invasion and angiogenesis in the central nervous system. *Front. Biosci.* 8, e289–e304.
- Zheng, X., Wise, S.M., Cristini, V., 2005. Nonlinear simulation of tumor necrosis, neo-vascularization and tissue invasion via an adaptive finite-element/level-set method. *Bull. Math. Biol.* 67, 211–259.